Parahydrogen-Induced ^{13}C Hyperpolarizer Using a Flow Guide for Magnetic Field Cycling to Evoke ^{1}H-^{13}C Spin Order Transfer Toward Metabolic MRI

Koudai Sawami, Tatsuya Naganuma, Hana Yabe, Toshihiko Taki, Neil J. Stewart, Yoshiki Uchio, Norihiko Takeda, Noriyuki Hatae, Takuya Hashimoto, Hiroshi Hirata, and Shingo Matsumoto

***Abstract*—*Objective:* The pair-wise addition of parahydrogen, the singlet form of molecular hydrogen, to unsaturated precursors evokes the hyperpolarization of two parahydrogen-derived ^{1}H nuclear spins through a process known as parahydrogen-induced polarization (PHIP). Subsequent spin order transfer (SOT) from the ^{1}H to the surrounding ^{13}C nuclear spins via magnetic field cycling (MFC) results in substantial signal enhancement in ^{13}C magnetic resonance imaging (MRI). Here, we report the development of a unique PHIP ^{13}C hyperpolarizer system using a flow guide for MFC. *Methods:* The optimal MFC scheme for ^{1}H to ^{13}C spin order transfer was quantum-chemically simulated using the J-coupling values of ^{13}C-labeled metabolic tracers. The flow guide system was three-dimensionally designed based on the simulated MFC scheme and premeasured magnetic field distribution in a zero-field chamber. *Results:* The system efficiently transfers the spin order of hyperpolarized ^{1}H to a particular ^{13}C spin when the parahydrogenated tracer passes through the flow guide at a designated flow rate. The ^{13}C MRI signal is enhanced more than 40,000 times in ^{13}C-labeled pyruvate and fumarate, compared to the thermal equilibrium level at 1.5 T, was achieved for conducting *in vivo* metabolic MRI of mice. *Conclusion:* A fully automated PHIP-based ^{13}C polarizer was developed using a unique flow guide to conduct the MFC for ^{1}H to ^{13}C SOT. Significance: The PHIP hyperpolarizer with a flow guide can conduct efficient ^{1}H-^{13}C SOT without a MFC magnetic field sweep system and offers a cost-effective alternative to conventional dynamic nuclear polarization.**

***Index Terms*—Flow guide, hyperpolarized ^{13}C MRI, magnetic field cycling, metabolism, PHIP.**

Manuscript received 11 August 2023; revised 6 January 2024; accepted 6 February 2024. Date of publication 13 February 2024; date of current version 20 June 2024. This work was supported in part by AMED under Grant JP20hm0102061 and Grant JP23gm6910009 and in part the Japan Society for the Promotion of Science (JSPS) KAKENHI under Grant JP20H00654 and Grant JP22K18435. *(Corresponding author: Shingo Matsumoto.)*

Koudai Sawami, Hana Yabe, Toshihiko Taki, and Yoshiki Uchio are with the Division of Bioengineering and Bioinformatics, Graduate School of Information Science and Technology, Hokkaido University, Japan.

Tatsuya Naganuma is with the R&D Department, Japan REDOX Ltd., Japan.

Neil J. Stewart is with the Division of Bioengineering and Bioinformatics, Graduate School of Information Science and Technology, Hokkaido University, Japan, and also with the POLARIS, Imaging Sciences, Department of Infection, Immunity & Cardiovascular Disease, University of Sheffield, U.K.

Norihiko Takeda is with the Division of Cardiology and Metabolism, Center for Molecular Medicine, Jichi Medical University, Japan.

Noriyuki Hatae is with the Division of Pharmaceutical Chemistry, School of Pharmacy, Yokohama University of Pharmacy, Japan.

Takuya Hashimoto is with the Molecular Synthesis and Function Laboratory, RIKEN Cluster for Pioneering Research, Japan.

Hiroshi Hirata is with the Division of Bioengineering and Bioinformatics, Faculty of Information Science and Technology, Hokkaido University, Japan.

Shingo Matsumoto is with the Division of Bioengineering and Bioinformatics, Faculty of Information Science and Technology, Hokkaido University, Sapporo 060-0808, Japan (e-mail: smatsumoto@ist.hokudai.ac.jp).

This article has supplementary downloadable material available at https://doi.org/10.1109/TBME.2024.3365195, provided by the authors.

Digital Object Identifier 10.1109/TBME.2024.3365195

I. Introduction

HYPERPOLARIZATION of heteronuclear spins such as ^{13}C and ^{15}N is a rapidly developing field of molecular imaging wherein nuclear magnetic resonance (NMR) and magnetic resonance imaging (MRI) signals can be transiently enhanced more than 10000 times compared to that at thermal equilibrium level. This enhancement allows for the noninvasive and real-time monitoring of metabolic reactions of ^{13}C or ^{15}N labeled tracers in the body [1], [2], [3], [4]. Hyperpolarization-evoking methodologies can be roughly classified into three types: brute force, dynamic nuclear polarization (DNP), and parahydrogen-induced polarization (PHIP) [5]. Among the three, DNP is the most successful and widely-used technique in metabolic MRI studies including clinical trials [6], [7]. However, DNP-based heteronuclear hyperpolarizers typically use a superconductive magnet of over 3 T in strength and microwave irradiation at a cryogenic temperature of approximately 1 K; such expensive requirements may be a major factor impeding their adoption into this promising research field.

PHIP is an older technique whose physical phenomena were first discovered in the late 1980s and has been recently regained attention as an alternative to DNP for hyperpolarized (HP) ^{13}C

MRI [8], [9], [10], [11]. In PHIP experiments, the hydrogenation of an unsaturated precursor with parahydrogen, the singlet form of molecular hydrogen, results in the generation of two HP ^{1}H nuclear spins, wherein the spin order is transferred to the surrounding ^{13}C nuclei using either NMR techniques such as Insensitive Nuclei Enhanced by Polarization Transfer (INEPT)-type pulse sequences or magnetic field cycling (MFC) [12], [13], [14].

Typical ^{1}H to ^{13}C spin order transfer (SOT) via MFC is a two-step process: rapid and diabatic drop down of magnetic field from earth field to zero field (<100 nT), and subsequent slow adiabatic re-magnetization within a magnetic shielding. The optimal MFC pattern to achieve the highest ^{13}C polarization for a particular ^{1}H-^{13}C SOT depends on the heteronuclear spin-spin coupling (J-coupling) network of nuclear spins in the ^{13}C-labeled tracer molecule. The MFC process is usually controlled by a magnetic field sweep coil placed inside the magnetic shielding [15], [16], [17]. Although the experimental MFC setup by magnetic sweeping is relatively simple compared to NMR-based SOT techniques and sufficiently efficient for a small sample volume (∼1 mL) in NMR measurements or HP ^{13}C MRI studies of a mouse, its efficiency might be diminished when preparing large-volume high-concentration samples over 100 mL and 100 mM, respectively, that would usually be required for clinical applications. The required accuracy of magnetic field strength for efficient ^{1}H-^{13}C SOT by MFC is below 100 nT, an order of one hundredth of the geomagnetic field. A few hundred cm^{3} container volume with such high homogeneity of a very low magnetic field in the zero-field chamber and magnetic field sweep coil is not easy to accomplish, limiting the clinical translation of PHIP-based hyperpolarized ^{13}C MRI.

In this study, we develop a parahydrogen-induced ^{13}C polarizer based on a unique MFC protocol, a flow guide system, to evoke ^{1}H-^{13}C SOT, which can avoid the coil-based magnetic field sweeping requirement for MFC-based SOT. Consequently, it may be suitable for preparing large volume of HP ^{13}C-labeled metabolic tracer solution via PHIP.

II. Parahydrogen-Induced ^{13}C Polarizer System Development

A. Design and Components of PHIP ^{13}C Hyperpolarizer With a Flow Guide

Fig. 1 illustrates the block diagram of the developed PHIP hyperpolarizer. The hydrogenation unit consists of a reaction chamber, reaction temperature control system, and gas pressure control systems, which mixes an unsaturated ^{13}C-labeled imaging tracer precursor with pressurized parahydrogen gas and a homogenous hydrogenation catalyst, resulting in the production of two HP ^{1}H nuclear spins (Fig. 2). The SOT unit transfers the spin order of the HP ^{1}H nuclei to the labeled ^{13}C nucleus via MFC. The fluid control unit conducts the switching of the parahydrogen and nitrogen gas via solenoidal valves and rotary valves. Thus, it manages most of the polarization process including precursor mixture charge, supply of parahydrogen gas for hydrogenation reaction, and transfer through the SOT units at the designated flow rate. All these processes are controlled by a microcomputer PSoC. Optional accessories can be added and automatically controlled by the PSoC and a software interface for chemical post-processes such as hydrolysis, neutralization, and filtration of hydrogenation catalysts and other side products. Fig. 3 contains images of the functional units of the polarizer. A parahydrogen generator is required in addition and is independent of the polarizer system (details are provided in the Supporting Information).

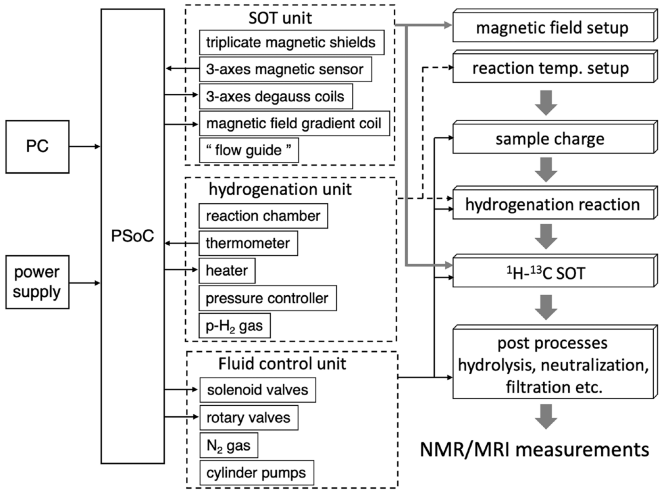

Fig. 1. Block diagram of the PHIP ^{13}C hyperpolarizer system. The PHIP ^{13}C hyperpolarizer primarily comprises three components: hydrogenation, SOT, and fluid control units. The hydrogenation unit controls the parahydrogenation reaction to produce two HP ^{1}H spins. The SOT unit precisely generates small magnetic field gradients inside the magnetic shield required to induce ^{1}H-^{13}C spin order transfer. The fluid control unit transfers sample solution to the next production steps. All timing is controlled with a microcomputer PSoC and software interface coded in C++.

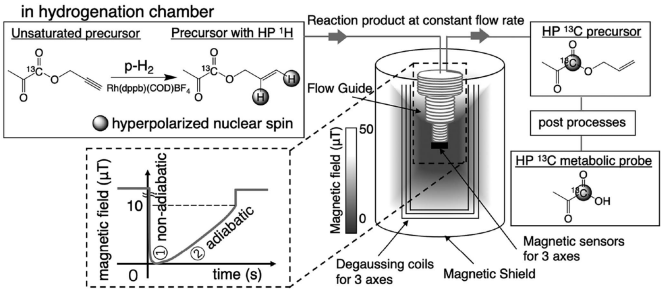

Fig. 2. Schematic diagram of HP ^{13}C-labeled metabolic probe solution production using the PHIP hyperpolarizer system. Parahydrogenation of the unsaturated precursor molecule produce two ^{1}H spins. The optimal MFC scheme is quantum mechanically simulated using J-coupling constants of the parahydrogenated precursor. The zero-field chamber comprises three layers of μ-metal cylinders, three degaussing coils for each of the 3 axes (solenoid coil for the z-axis and two saddle coils for the x and y axes), and a 3-axis magnetic sensor placed around the center of the zero-field chamber. An optional magnetic field gradient coil can be used for fine adjustment of the gradient slope if required. Based on the magnetic field distribution within the zero-field chamber, the flow path pattern in the flow guide is designed to ensure that the parahydrogenation product receives optimal MFC for ^{1}H-^{13}C spin order transfer when passing through the flow guide at a constant flow rate. HP ^{13}C metabolic probe solution is finally generated after additional post processes such as side-arm hydrolysis, neutralization, and filtration.

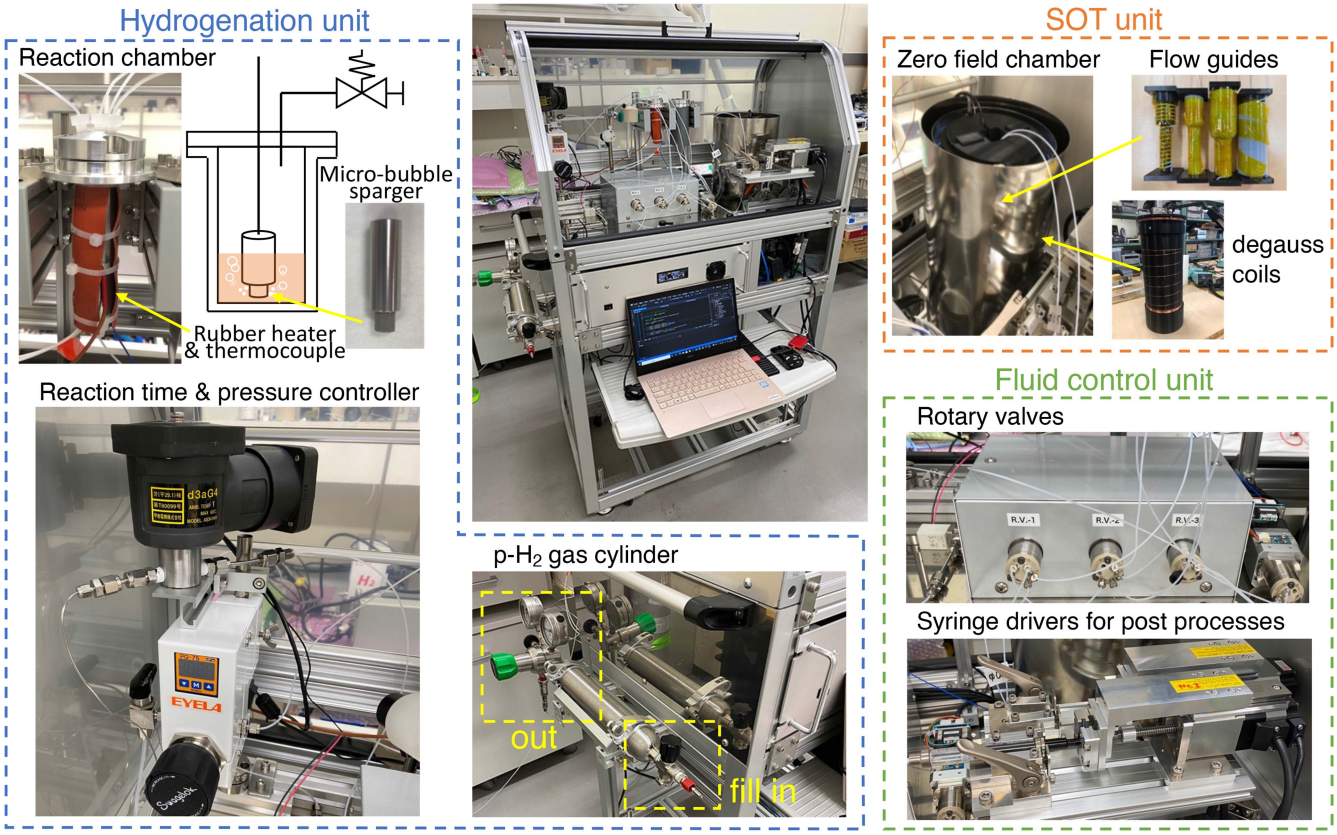

Fig. 3. Images of the portable PHIP ^{13}C hyperpolarizer system using a flow guide for ^{1}H-^{13}C SOT. The adiathermanous coverage was temporally removed to allow easy visualization of the reaction chamber components.

B. Parahydrogenation Reactor Unit

Three different sizes of lab-made hydrogenation reaction chambers with inner volumes of 19.4, 55.3, and 190.2 cm^3, were made of aluminum and connected by upper four 1/16" tubing lines for precursor sample charge, parahydrogen gas bubbling, pressure controller, nitrogen gas inlet, and hydrogenated sample outlet to the SOT unit at the bottom of the reaction chamber. Different sizes (surface area) of spargers with 2 µm holes for micro-bubbling were fixed at the end of the parahydrogen gas inlet line. The reaction chamber was wrapped with a rubber heater, and a thermocouple was placed between the heater and outside wall of the reaction chamber to monitor and control of hydrogenation reaction temperature. While the reaction chamber is usable at higher gas pressures, the maximum experimental pressure of both the parahydrogen and nitrogen gasses was set at 1.0 MPa because of the limit imposed by the local regulation of the research facility.

C. SOT Unit With Flow Guide for MFC

Parahydrogenation reactions occurring on carbon multiple bonds lead to the production of two hyperpolarized ^{1}H spins. Immediately after their generation, the spin order of these hyperpolarized ^{1}H spins spread to neighboring nuclear spins, influenced by the J-coupling network within the molecule and the magnetic field, i.e., Larmor frequencies of ^{1}H and ^{13}C. In other words, adjusting the varying magnetic field allows for the efficient transfer of spin order from the hyperpolarized ^{1}H spins to the labeled ^{13}C spin. To accomplish this magnetic field change, known as MFC, for ^{1}H-^{13}C SOT, we devised and implemented a small field gradient within the magnetic shield and three-dimensional (3D) fluid path. This design ensures that the precursor molecule, containing two hyperpolarized ^{1}Hs, undergoes the optimal MFC for ^{1}H-^{13}C SOT as it passes through the 3D fluid path subjected to the field gradient.

The SOT unit consists of a three-layered μ-metal magnetic shield (ZG-206 from Magnetic Shield Corp., USA), three-axis degaussing coils, a field gradient adjustment coil (anti-Helmholtz coil pair along the long axis of the magnetic shield), flow guide, and three-axis magnetic sensor (Mag619U, Bartington Instruments, U.K.) placed at the bottom of the flow guide, just below the zero-field point (Fig. 2). The top of the magnetic shield was kept open to generate an ultrasmall magnetic field gradient, approximately 1.2 µT/cm, from the zero-field point around the center to the upper edge of the magnetic shield (Supporting Fig. 2). The slope of the magnetic field gradient could be finely adjusted by varying the current of the field gradient adjustment coil. Based on the pre-measured magnetic field distribution inside the magnetic shield, the 3D fluid path flow guide was designed and created by winding a PTFE tubing (ID 0.5 mm, OD 1/16") around a resin holder made with a 3D printer, such that the parahydrogenated metabolic tracer containing the

hyperpolarized singlet ^{1}H pair receives the optimal MFC profile when the sample passes through the flow guide placed in the magnetic shield. The typical MFC pattern for ^{1}H-^{13}C SOT is a combination of rapid (<100 ms) diamagnetic drop down of the magnetic field from a point at over 10 μT to the zero-field point below 100 nT, followed by slow adiabatic re-magnetization to 10 μT over 1–5 s, with exact timings dependent on the chemical structure of the ^{13}C labeled metabolic tracer. The details of the quantum mechanical simulation of the optimal MFC profile using the J-coupling constants of the tracer have been previously described [15], [18]. To obtain such an MFC profile, the flow guide moves the parahydrogenated sample directly through a straight fluid path from the upper edge of the magnetic shield to the zero-field point for diabatic change and then moves the sample slowly back to the edge of the magnetic shield for adiabatic remagnetization via a winding fluid path. Of note, different flow guides are required for different precursor molecules to be hyperpolarized.

D. Post Process Unit

After spin order transfer of the two HP ^{1}Hs to the target ^{13}C spin, additional processes such as chemical modification, neutralization, phase separation, and filtering of the hydrogenation catalyst and other side products, are typically required for biomedical applications, including HP ^{13}C metabolic MRI studies. Optional accessories for post processing, such as syringe drivers to add a hydrolysis/neutralization solution (lower right in Fig. 3), can be easily added to the polarizer system and controlled from the same interface using the PSoC control board.

III. Materials and Methods

A. Preparation of HP [1-^{13}C] pyruvate Solution

The reaction mixture for HP [1-^{13}C]pyruvate was prepared as follows: a precursor of [1-^{13}C]propargylpyruvate was synthesized according to the method reported by Chukanov et al. [19]. [1-^{13}C]propargylpyruvate (20 μL) and hydrogenation catalyst [Rh(dppb)(COD)]BF_4 (20 mg, #341134, Sigma-Aldrich, St Louis, MO) were dissolved in 1 mL chloroform in a glovebox under argon atmosphere (<0.5% O_2). The mixture was centrifuged at 15000 rpm for 5 min to remove impurities and the supernatant was used for parahydrogenation reaction. The precursor mixture solution was set in the polarizer system, which automatically (i) transfers the solution to the reaction chamber, (ii) performs parahydrogenation reaction at 55–60 °C for 10 seconds at 0.60 MPa of parahydrogen gas pressure (unless mentioned otherwise), (iii) facilitates ^{1}H-^{13}C SOT in a zero-field chamber using the flow guide system, (iv) mixes the solution with 0.9 mL of hydrolysis solution containing 62.5 mM NaOD, 50 mM Tris-HCl, and 0.5 mM EDTA-2Na in D_2O, and (v) performs nitrogen gas bubbling at 75 °C for 10–12 seconds on a heat block to vaporize chloroform and allylalcohol generated by hydrolysis (catalyst is precipitated during this procedure), thereby manufacturing approximately 0.6 mL aqueous solution containing 80–90 mM hyperpolarized [1-^{13}C]pyruvate. The pH of the final solution was 7.0–8.5. The parahydrogen gas cylinder was pressure-regulated and set at 0.8 MPa against a pressure limiter at 0.6 MPa in the hydrogenation reaction chamber using a pressure controller (#BPR-1000, EYELA, Tokyo, Japan). This 0.2 MPa pressure difference ensures sufficient flow of pressurized parahydrogen gas required for efficient parahydrogenation reaction.

B. Ex Vivo and in Vivo HP ^{13}C MRI Experiments

All animal experiments were performed following the guidelines of the Law for the Care and Welfare of Animals in Japan and approved by the Animal Experiment Committee of Hokkaido University (Approval No. 21–0007). In *ex vivo* and *in vivo* experiments, HP [1-^{13}C]pyruvate solutions were prepared by using the smallest hydrogenation reaction chamber with inner volume of 19.4 cm^3.

Ex vivo MR spectroscopy of the metabolic reaction of HP [1-^{13}C]pyruvate with tumor tissue homogenate was performed on a home-built 1.5 T permanent magnet MRI system with a multinuclear spectrometer (Medalist, Japan REDOX Ltd.). Solid murine SCCVII tumors were generated by injecting 5×10^5 cells subcutaneously into the right hind leg of female C3H/HeJYokSlc mice (Japan SLC Inc., Shizuoka, Japan). When the tumors grew to approximately 1.2 cm in size, the tumor tissues were excised and frozen in a deep freezer at −80 °C until use. One volume of tumor tissue was homogenized in 9 volumes of PBS, and 0.3 mL homogenate solution was placed in a 3.5 mL chemical vial containing NADH as a cofactor of lactate dehydrogenase (LDH) solved in 50 μL PBS for a final concentration of 50 mM. 0.8 mL HP [1-^{13}C]pyruvate solution was infused into the SCCII tumor homogenate/NADH mixture by an injection through 1/16" OD PTFE tubing from a syringe outside the magnet gap. Dynamic ^{13}C spectra were acquired over a period of 4–5 minutes until the [1-^{13}C]pyruvate signal was undetectable. The MR spectroscopy parameters were set as follows: Repetition Time (TR) = 2 s; flip angle = 10°; spectral bandwidth = 122 ppm, centered on the [1-^{13}C]pyruvate resonance.

An *in vivo* HP ^{13}C MRI study of pyruvate metabolism in healthy C57BL/6NCrSlc mice (Japan SLC Inc., Shizuoka, Japan) was conducted using the same 1.5 T MRI system with a Japan REDOX spectrometer in combination with home-built RF coils comprising of an inner solenoid coil for ^{13}C channel and an outer saddle coil for ^{1}H channel. *In vivo* imaging experiments were performed using a 2D spatially phase-encoded ^{13}C chemical shift imaging (CSI) pulse sequence with centric k-space data acquisition. Typical parameters were set as follows: 16×16 matrix; FOV = 32 × 32 mm; TE/TR = 10/75 ms; flip angle = 10°; spectral bandwidth = 2 kHz (122.4 ppm) for 128 points. HP [1-^{13}C]pyruvate (80–90 mM, 10 μL/g body weight) was injected through the tail vein over the course of 12 seconds via a plastic cannula connected to a syringe outside the magnet bore via PE10 tubing. To denoise the 3D CSI image data, the rank reduced image matrices were generated by tensor decomposition with a small core-tensor size as described previously [20]. The size of the core-tensor, which corresponds to the rank of the CSI image matrices, was set to 8 and 12 for each spatial and spectral dimension, respectively. The CSI images were zero-filled and

reconstructed with a matrix size of 64 × 64. Brain images were displayed as parametric maps of metabolite ratios with a mask obtained from an anatomical ^{1}H MRI.

IV. Results and Discussion

A. Polarization Setup and Portability

After the first successful *in vivo* application of PHIP to HP ^{13}C MRI reported by Golman et al. in 2001, parahydrogen-induced hyperpolarization techniques for developing biomedical or clinical polarizers have progressed rapidly [21]. Such advances include automation, tracer development, PHIP side-arm hydrogenation, reversible exchange (SABRE), SOT techniques, and purification methods [12], [14], [22], [23], [24], [25]. A practical advantage of PHIP-based polarizers over conventional DNP polarizers is their portability. A typical DNP polarizer consists of superconductive magnet that is difficult to move and occupies space near the MRI room. The PHIP polarizer developed in this study is designed to sit near the MRI scanner only when conducting a hyperpolarization study.

After the system was switched on, the hydrogenation reactor required approximately 6 min to achieve the target reaction temperature, which is the most time-consuming step (Fig. 4). The automatic adjustment of the zero-field and magnetic field gradient inside the zero-field chamber was completed within 1 min with an accuracy of less than 10 nT. To investigate the effect of magnetic field leak from our NMR and MRI systems, located in different rooms, on the zero-field adjustment of the polarizer, we moved the portable polarizer between the NMR and MRI rooms. The zero-field setup time and magnetic field strength at the center of the magnetic shielding were measured when placed within 2–3 m of a benchtop 1.4 T NMR scanner and 1.5 T preclinical permanent magnet MRI scanner. The zero-field setup time was near identical, however the magnetic field strength around the center of the magnetic shielding was slightly (few nT) higher when placed near the MRI than the benchtop NMR scanner (Fig. 4(b) and (c)). This difference may be due to the fringe magnetic field of the MRI magnet. Additionally, this residual magnetic field inside of the zero-field chamber became larger if the polarizer was placed closer to the MRI scanner. These results confirm that the developed PHIP ^{13}C polarizer has the potential to be moved to near the MRI scanner only when used and can be operated within 6 min after turning on the system.

B. Preparation of Large Volume of HP ^{13}C Tracer Solution

Considering the typical clinical dose of 0.1 mmol/kg of HP [1-^{13}C]pyruvate in clinical studies with the DNP polarizers, manufacturing at least 100 mL of 100 mM HP ^{13}C tracer solution is required for the clinical translation of PHIP polarizers. As an initial step towards clinical translation, we investigated the effect of scaling up the sample volume on the final ^{13}C polarization level.

Using a small hydrogenation reaction chamber with 19.4 cm^3 inner volume, the hydrogenation rate linearly increased with

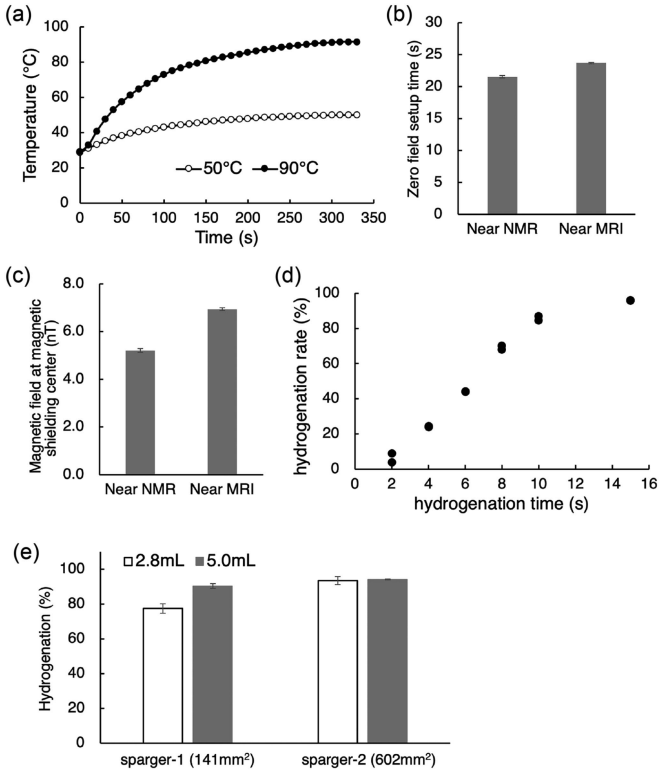

Fig. 4. Basic performance and portability evaluation of the PHIP ^{13}C polarizer. (a) The parahydrogenation reaction chamber requires 6 min to achieve the target temperature. (b) Zero field adjustment at the center of zero field chamber completes in 30 s (n = 2), and (c) residual magnetic field strength is less than 10 nT when placed the polarizer 2–3 m apart from either 1.4 T benchtop NMR or 1.5 T MRI system (n = 2). (d) Hydrogenation rate of [1-^{13}C]propargyl pyruvate linearly increases with the reaction time until 10 s, and (e) the larger size of micro-bubbling sparger for the parahydrogen gas inlet result in a better hydrogenation rate for the large volumed sample (n = 2).

parahydrogen bubbling time until 10 s (Fig. 4(d)). The hydrogenation rate showed no significant difference when the sample volume was increased up to 5 mL with either size of the micro-bubbling sparger for the parahydrogen gas inlet. ^{1}H and ^{13}C polarizations for 1 mL precursor solution volume of 78 mM propargyl-[1-^{13}C]pyruvate at the time of MRI scanning were 10.2 ± 0.48% and 7.4 ± 1.0%, respectively, resulting in an estimated ^{1}H-^{13}C SOT efficiency of 72.5% if ignored the relaxation time of singlet ^{1}H spin pair, approximately 29 s at the earth field. The ^{13}C polarization of the final product, [1-^{13}C]pyruvate, further decreased to 50–70% of that of allyl-[1-^{13}C]pyruvate during hydrolysis, neutralization, and purification processes. The ^{1}H and ^{13}C polarizations, SOT efficiency, and loss by side-arm cleavage were similar to those of MFC via coil-based magnetic field sweeping [26].

Further increase in precursor sample volume with larger sizes of hydrogenation reaction chamber (55.3 or 190.2 cm^3) resulted in diminished hydrogenation rate and corresponding ^{13}C polarization, as illustrated in Fig. 5. The loss of ^{13}C polarization in a large-scale sample can be attributed to two possible reasons. The first is fewer HP ^{1}H spins, the source of spin-order, because of the low hydrogenation rate. For a larger reaction chamber,

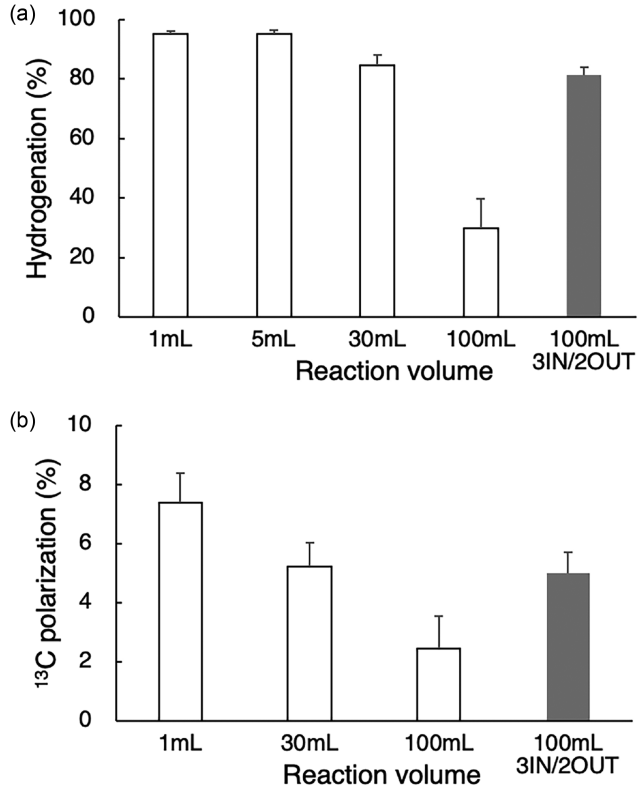

Fig. 5. (a) Hydrogenation rate and (b) ^{13}C polarization of different volumes of [1-^{13}C]propargyl pyruvate solution. Both hydrogenation rate and ^{13}C polarization decreased with increasing sample volume when using a single inlet for parahydrogen gas and single outlet of parahydrogenated product and increased when using a reaction chamber with 3 inlets and 2 outlets (grey bar) . n = 2 for each volume.

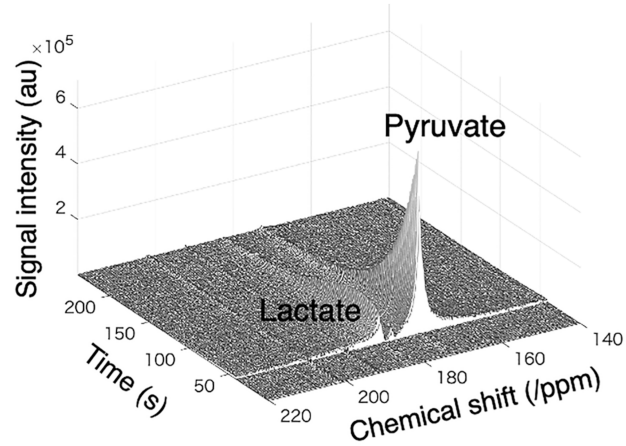

Fig. 6. *Ex vivo* metabolic reaction of HP ^{13}C pyruvate produced by the PHIP hyperpolarizer system as measured by a benchtop NMR. Dynamic ^{13}C NMR spectra of HP [1-^{13}C]pyruvate mixed with mouse tumor homogenate resulted in the generation of HP [1-^{13}C]lactate at 184 ppm.

TABLE I
DURATIONS AND POLARIZATIONS IN *IN VIVO* EXPERIMENTS

Process	Duration (s)	Polarization (%)
parahydrogenation	11	$P_{1H} > 10.2$ [a]
^{1}H-^{13}C SOT	6	$P_{13C} > 7.4$ [a]
hydrolysis & neutralization	22	
injection	12	$P_{13C} = 5.1$ [b]
wait for distribution	13	
CSI acquisition	19	

[a] polarization of allyl-[1-^{13}C]pyruvate, [b] polarization of [1-^{13}C]pyruvate.

achieving the target parahydrogen pressure of 0.6 MPa after parahydrogen gas bubbling initiation requires more time; this process takes less than 5 s for the smallest 19.4 cm^3 chamber and over 10 s for the larger chambers. This implies that the target pressure is not achieved if the hydrogenation reaction time is 10 s. Further, the mixing efficiency of the precursor solution with parahydrogen gas is low in the presence of only one inlet for a 100 mL solution compared with less than 5 mL of the sample solution. A second reason for ^{13}C polarization loss may be the relaxation of HP ^{13}C spins during solution removal from the reaction chambers through the 1/16-inch tubing line by pressurized N_2 gas. Only a few seconds were required to remove 1 mL of HP ^{13}C tracer solution, whereas more than 1 min was required to remove 100 mL solution. To confirm this, we created a new large reaction chamber with three parahydrogen inlets and two solution outlets, resulting in substantial improvements in the hydrogenation rate (81.5 $\pm$ 2.6%), ^{1}H and ^{13}C polarization of allyl-[1-^{13}C]pyruvate (7.5 $\pm$ 1.0% and 5.0 $\pm$ 0.7%, respectively; Fig. 5 grey bars). These results suggest the potential of the PHIP ^{13}C polarizer with a flow-guided MFC system to scale up its production ability to human size for clinical translation. The maximum production quantity of HP [1-^{13}C]pyruvate using our current system is approximately 10 mmol with a concentration of 80 mM in 126 mL.

C. Feasibility Study of Biomedical Applications

In DNP studies, HP [1-^{13}C]pyruvate has been successfully used to detect metabolic alteration in various disease models, and clinical studies involving hundreds of patients, most of whom were cancer patients, have been conducted in more than 10 facilities worldwide [5], [6], [7]. To investigate whether HP [1-^{13}C]pyruvate prepared by PHIP functions comparably as a metabolic imaging probe, HP [1-^{13}C]pyruvate was mixed with murine tumor homogenates. Time-dependent peak generation of [1-^{13}C]lactate, a metabolic product of LDH from pyruvate, was observed at 184 ppm immediately after the infusion of HP [1-^{13}C]pyruvate with NADH (Fig. 6), and the [1-^{13}C]pyruvate and lactate signals lasted for up to 5 min.

To demonstrate the feasibility of the *in vivo* metabolic imaging of HP [1-^{13}C]pyruvate produced by the developed PHIP polarizer system, CSI sequence was performed on the heads and abdomens of mice using a 1.5 T MRI scanner. The durations required for each step to generate the HP [1-^{13}C]pyruvate and the ^{1}H or ^{13}C polarization values at each respective step in *in vivo* experiments were summarized in Table I. The distribution of HP [1-^{13}C]pyruvate and bicarbonate, a metabolite reflecting the flux to oxidative phosphorylation, 25 sec after injection showed a strong signal in the kidney region, whereas that of [1-^{13}C]lactate

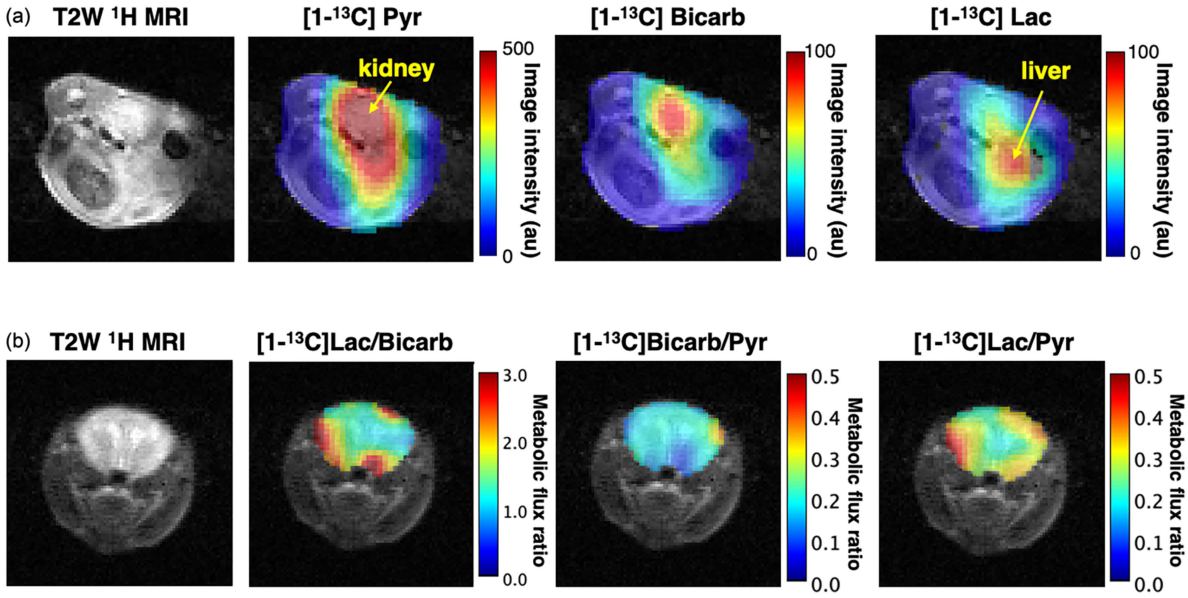

Fig. 7. In vivo CSI of HP [1-^{13}C]pyruvate metabolism in healthy mice. (a) Maps of T_2-weighted ^{1}H MRI, HP ^{13}C pyruvate, bicarbonate, and lactate at the mouse abdomen. (b) Maps of T_2-weighted ^{1}H MRI and metabolic flux ratios of HP ^{13}C lactate/bicarbonate, bicarbonate/pyruvate, and lactate/pyruvate at the mouse brain. Bicarb, Lac, Pyr denote bicarbonate, lactate, and pyruvate, respectively.

exhibited a strong signal in the liver region, as illustrated in Fig. 7(a). Notably, a peak was recognizable at approximately 178 ppm in the ^{13}C spectrum of liver pixels, indicating the metabolic flux to alanine, but it was inseparable *in vivo* from the large pyruvate peak by our 1.5 T MRI scanner with a permanent magnet due to the limited homogeneity of the magnetic field. By normalizing the signal intensities of the bicarbonate and lactate peaks to that of the pyruvate peak, parametric maps reflecting the fluxes from pyruvate to each metabolite were produced in the mouse brain region (Fig. 7(b)). A parametric map of the lactate-to-bicarbonate ratio was also produced in the brain image, which is a well-known imaging marker that indicates a metabolic shift between oxidative phosphorylation and glycolysis in various diseases. Slight image distortions were observed in the hyperpolarized ^{13}C CSI images. The hyperpolarized ^{13}C signal rapidly diminishes dependent on the longitudinal (T_1) relaxation time of hyperpolarized ^{13}C spin, the flip angle of the excitation pulse, and the applied field gradients for imaging. This leads to spatial distortion in the reconstructed image after a two-dimensional Fourier transformation. Additional information about the image distortion is provided in the Supporting Fig. 4.

In addition to pyruvate, the PHIP polarizer can produce HP [1-^{13}C]fumarate. Details of the preparation of HP [1-^{13}C]fumarate solution and representative images of its application to visualize necrotic cell death in the livers of mice with acetaminophen-induced liver failure are available in the Supporting Information. Collectively, these results clearly demonstrate the feasibility of the developed PHIP-based ^{13}C hyperpolarizer system for metabolic MRI.

V. Conclusion

In this work, we have developed a PHIP-induced ^{13}C hyperpolarization system for ^{1}H -^{13}C SOT using a flow guide placed under an ultrasmall magnetic field gradient within a zero-field chamber. The efficiency of ^{1}H-^{13}C SOT with a flow guide is 72.5%, resulting in a ^{13}C polarization of [1-^{13}C]pyruvate of 5.1% and 3.0% for small ($<$ 1.0 mL) and large ($>$ 100 mL) sample volumes at a concentration of 80 mM. For a comparison with other parahydrogen polarizers, a comprehensive review is available in reference [24]. Although a large hydrogenation reaction chamber with multiple inlets and outlets is promising as a scalable route to produce a clinical dose of HP ^{13}C tracer solution, several 30–50 mL chambers in parallel and bundled outlet tubes into the flow guide for SOT might be a more practical choice for preparing large-volume samples than using a single large ($>$100 mL) reaction chamber. In addition, we have demonstrated the feasibility of *in vivo* MRI of PHIP-polarized [1-^{13}C]pyruvate metabolism in mice, which is similar to conventional DNP-type polarizers. These findings should facilitate further biomedical applications and the eventual clinical translation of parahydrogen-induced polarization techniques.

References

[1] K. Golman et al., "Real-time metabolic imaging," *Proc. Nat. Acad. Sci. USA*, vol. 103, no. 30, pp. 11270–11275, Jul. 2006.

[2] H. Park and Q. Wang, "State-of-the-art accounts of hyperpolarized (15)n-labeled molecular imaging probes for magnetic resonance spectroscopy and imaging," *Chem. Sci.*, vol. 13, no. 25, pp. 7378–7391, Jun. 2022.

[3] N. J. Stewart et al., "Hyperpolarized (13)c magnetic resonance imaging as a tool for imaging tissue redox state, oxidative stress, inflammation, and cellular metabolism," *Antioxidants Redox Signaling*, vol. 36, no. 1/3, pp. 81–94, Jan. 2022.

[4] S. Matsumoto et al., "Metabolic and physiologic imaging biomarkers of the tumor microenvironment predict treatment outcome with radiation or a hypoxia-activated prodrug in mice," *Cancer Res.*, vol. 78, no. 14, pp. 3783–3792, Jul. 2018.

[5] N. J. Stewart and S. Matsumoto, "Biomedical applications of the dynamic nuclear polarization and parahydrogen induced polarization techniques for hyperpolarized (13)c mr imaging," *Magn. Reson. Med. Sci.*, vol. 20, no. 1, pp. 1–17, Mar. 2021.

[6] R. Woitek and F. A. Gallagher, "The use of hyperpolarised (13)c-mri in clinical body imaging to probe cancer metabolism," *Brit. J. Cancer*, vol. 124, no. 7, pp. 1187–1198, Mar. 2021.

[7] S. J. Nelson et al., "Metabolic imaging of patients with prostate cancer using hyperpolarized [1-(1)(3)c]pyruvate," *Sci. Transl. Med.*, vol. 5, no. 198, Aug. 2013, Art. no. 198ra108.

[8] C. R. Bowers and D. P. Weitekamp, "Transformation of symmetrization order to nuclear-spin magnetization by chemical reaction and nuclear magnetic resonance," *Phys. Rev. Lett.*, vol. 57, no. 21, pp. 2645–2648, Nov. 1986.

[9] C. R. Bowers and D. P. Weitekamp, "Parahydrogen and synthesis allow dramatically enhanced nuclear alignment," *J. Amer. Chem. Soc.*, vol. 109, no. 18, pp. 2645–2648, 1987.

[10] N. J. Stewart et al., "Hyperpolarized (13) c magnetic resonance imaging of fumarate metabolism by parahydrogen-induced polarization: A proof-of-concept in vivo study," *ChemPhysChem*, vol. 22, no. 10, pp. 915–923, May 2021.

[11] M. Gierse et al., "Parahydrogen-polarized fumarate for preclinical in vivo metabolic magnetic resonance imaging," *J. Amer. Chem. Soc.*, vol. 145, no. 10, pp. 5960–5969, Mar. 2023.

[12] F. Reineri et al., "Parahydrogen induced polarization of 13c carboxylate resonance in acetate and pyruvate," *Nature Commun.*, vol. 6, Jan. 2015, Art. no. 5858.

[13] A. Svyatova et al., "Phip hyperpolarized [1-(13)c]pyruvate and [1-(13)c]acetate esters via ph-inept polarization transfer monitored by (13)c nmr and mri," *Sci. Rep.*, vol. 11, no. 1, Mar. 2021, Art. no. 5646.

[14] J. B. Hovener et al., "Pasadena hyperpolarization of 13c biomolecules: Equipment design and installation," *Magn. Reson. Mater. Phys., Biol. Med.*, vol. 22, no. 2, pp. 111–121, Apr. 2009.

[15] N. J. Stewart et al., "Long-range heteronuclear j-coupling constants in esters: Implications for (13)c metabolic MRI by side-arm parahydrogen-induced polarization," *J. Magn. Reson.*, vol. 296, pp. 85–92, Nov. 2018.

[16] J. Eills et al., "Real-time nuclear magnetic resonance detection of fumarase activity using parahydrogen-hyperpolarized [1-(13)c]fumarate," *J. Amer. Chem. Soc.*, vol. 141, no. 51, pp. 20209–20214, Dec. 2019.

[17] B. Joalland et al., "Pulse-programmable magnetic field sweeping of parahydrogen-induced polarization by side arm hydrogenation," *Anal. Chem.*, vol. 92, no. 1, pp. 1340–1345, Jan. 2020.

[18] E. Cavallari et al., "Effects of magnetic field cycle on the polarization transfer from parahydrogen to heteronuclei through long-range j-couplings," *J. Phys. Chem. B*, vol. 119, no. 31, pp. 10035–10041, Aug. 2015.

[19] N. V. Chukanov et al., "Synthesis of unsaturated precursors for parahydrogen-induced polarization and molecular imaging of 1-(13)c-acetates and 1-(13)c-pyruvates via side arm hydrogenation," *Amer. Chem. Soc. Omega*, vol. 3, no. 6, pp. 6673–6682, Jun. 2018.

[20] S. Kishimoto et al., "Imaging of glucose metabolism by 13c-mri distinguishes pancreatic cancer subtypes in mice," *Elife*, vol. 8, Aug. 2019, Art. no. e46312.

[21] K. Golman et al., "Parahydrogen-induced polarization in imaging: Sub-second (13)c angiography," *Magn. Reson. Med.*, vol. 46, no. 1, pp. 1–5, Jul. 2001.

[22] R. W. Adams et al., "Reversible interactions with para-hydrogen enhance nmr sensitivity by polarization transfer," *Science*, vol. 323, no. 5922, pp. 1708–1711, Mar. 2009.

[23] S. Knecht et al., "Rapid hyperpolarization and purification of the metabolite fumarate in aqueous solution," *Proc. Nat. Acad. Sci. USA*, vol. 118, no. 13, Mar. 2021, Art. no. e2025383118.

[24] A. B. Schmidt et al., "Instrumentation for hydrogenative parahydrogen-based hyperpolarization techniques," *Anal. Chem.*, vol. 94, no. 1, pp. 479–502, Jan. 2022.

[25] A. B. Schmidt et al., "Catalyst-free aqueous hyperpolarized [1-(13)c]pyruvate obtained by re-dissolution signal amplification by reversible exchange," *Amer. Chem. Soc. Sens.*, vol. 7, no. 11, pp. 3430–3439, Nov. 2022.

[26] F. Reineri et al., "Hydrogenative-phip polarized metabolites for biological studies," *Magn. Reson. Mater. Phys., Biol. Med.*, vol. 34, no. 1, pp. 25–47, Feb. 2021.